Metrological characterization of INRIM's Yb lattice clock

Metrological Characterization Of INRIM's Yb Lattice Clock

Benjamin Rauf*†, Marco Pizzocaro*, Pierre Thoumany*, Gianmaria Milani*†, Filippo Bregolin*†, Michele Gozzelino*, Davide Calonico*, Giovanni Antonio Costanzo*, Cecilia Clivati* and Filippo Levi*
*Istituto Nazionale di Ricerca Metrologica (INRIM), Physical Metrology Division
Strada delle Cacce 91, 10135 Torino, Italy
Email: b.rauf@inrim.it
†Politecnico di Torino, Dipartimento di Elettronica e Telecomunicazioni
C.so duca degli Abruzzi 24, 10125 Torino, Italy

***Abstract*— We present the results of a preliminary metrological characterization of our neutral ^{171}Ytterbium-atoms lattice clock at INRIM. During one clock cycle we cool and trap the atoms utilizing 399 nm laser light for the first stage magneto-optical trap (MOT), followed by a cooler 556 nm 2nd stage MOT. Atoms are then transferred in a one-dimensional, horizontal lattice adjusted to the magic wavelength (759 nm). Subsequently the clock transition at 578 nm is excited by a laser stabilized to an ultra-stable cavity, followed by repumping and state-detection. We obtain $2 \cdot 10^3$ atoms in the lattice after 150 ms of loading time. The laser radiation at 399 nm, 556 nm and 578 nm is produced via infrared lasers and non-linear crystals, whereas the lattice features a Titanium-Sapphire laser. A detailed description of the laser light generation and stabilization as well as of the the physics package is given. We locked the clock laser to the atoms and achieved a first metrological characterization through optical fiber-comb based comparison with INRIM's primary frequency standard, the IT-CsF2 cryogenic fountain clock [1]. The reported frequency of the clock transition agrees to the value recommended by the BIPM [2] within the stated uncertainty.**

I. Introduction

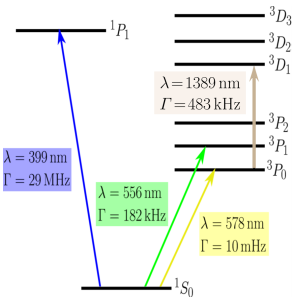

Fig. 1. The relevant atomic transitions in Yb for clock operation

In recent years atomic clocks based on optical transitions in ions or neutral atoms have surpassed the current standard for the SI-second, Cesium fountain clocks, by more than one order of magnitude in accuracy as well as in stability [3] and have therefore been recognised by the BIPM [2] as secondary representations of the second. Among these atomic frequency standards is the spin and angular-momentum forbidden and therefore long-living $^1S_0 \rightarrow {}^3P_0$ transition in neutral ^{171}Yb. The relevant atomic levels and transitions for cooling, trapping and interrogation of Yb are shown in Fig. 1. The fermionic ^{171}Yb isotope has a nuclear spin of I=1/2 leading to a hyperfine structure which makes it an interesting candidate not only as frequency standard, but also for quantum computing and quantum simulation. It's sensitivity to possible variations of the fine-structure constant make it also an interesting proposal for fundamental science. We are operating a ^{171}Yb based optical clock in the laboratories of INRIM. The cooling takes place in a two-stage MOT that utilizes the strong (linewidth 29 MHz) $^1S_0 \rightarrow {}^1P_1$ transition at 399 nm for trapping and the weaker $^1S_0 \rightarrow {}^3P_1$ transition (linewidth 182 kHz) subsequently cooling further down the atoms to few microkelvins. The atoms are then transferred to an optical lattice operating at the 759 nm magic wavelength. Excitation of the 578 nm $^1S_0 \rightarrow {}^3P_0$ clock-transition with a natural lifetime of more than 100 s is reversed by exploiting repumping through driving of the $^3P_0 \rightarrow {}^3D_1$ 1389 nm (linewidth 483 kHz) transition. With the experimental setup completed we have obtained locking on the spin-polarized clock transition and, by comparing to INRIM's IT-CsF2 Cs atomic fountain clock, recieved a preliminary chracterization of our clock.

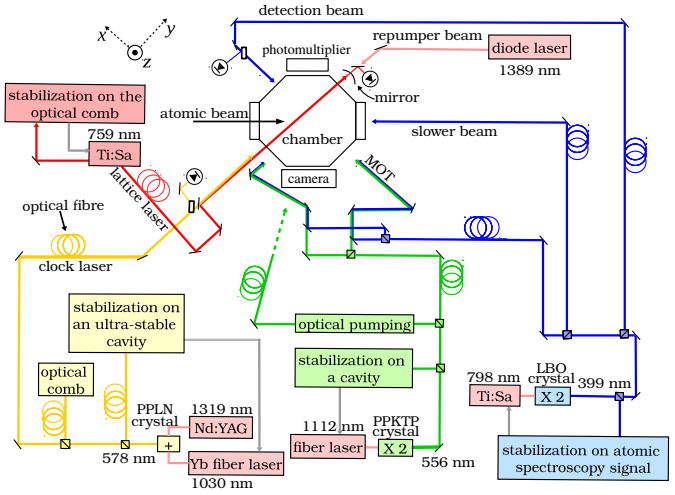

Fig. 2. Drawing of the vacuum chamber and optical composition

II. Experimental Setup

A. Physics package

Fig. 2 displays the vacuum chamber and its surrounding optical assembly for atomic spectroscopy. The atoms are emitted in a collimated beam by an effusion oven (Temperature 400°C). Instead of implementing a Zeeman-slower for maximum capture efficiency here the distance between atoms source

and trapping chamber is kept minimal for increased atomic flux. The atoms are trapped inside the custom aluminum chamber designed for wide optical access with indium-sealed viewports. 10 thermistors are distributed all over the chamber for precise blackbody-shift evaluation and it is being kept at ultra-high vacuum (pressure $< 10^{-9}$ mbar) by two ion pumps and one non-evaporable getter pump. The MOT coils are vertically arrayed outside the vacuum chamber. Three pairs of Helmholtz coils are compensating the stray magnetic field.

B. Laser ensemble

All lasers are spatially seperated from the vacuum chamber and are delivered to the it by means of polarization-maintaining (PM) optical fibers. The radiation at 399 nm acting on the $^1S_0 \rightarrow {}^1P_1$ transition is produced via 2nd harmonic generation (SHG) from a 798 nm Titanium-Sapphire (Ti:Sa) laser by means of a nonlinear lithium-triborate (LBO) crystal inside an enhancement cavity [4]. The Ti:Sa laser delivers an output power of about 1.1 W with an 8 W solid state pump laser at 532 nm with the typical total power of 399 nm radiation set to 0.5 W. The laser is locked to the $^1S_0 \rightarrow {}^1P_1$ transition through transverse spectroscopy of an auxiliary atomic beam. The 2nd stage MOT and the spin-polarizing beam are generated via SHG of an amplified 1112 nm Yb-doped fiber laser passing through a single-pass periodically-poled potassium titanyl phosphate (PPKTP) crystal. About 10 mW of 556 nm radiation are obtained from 1.0 W of infrared light. The laser is referenced to a stable cavity made out of Corning Ultra-Low Expansion glass (ULE). About 1 W of lattice power is provided by a Ti:Sa laser with an initial output of about 2 W. The 578 nm laser acting upon the clock transition is generated by sum-frequency-generation (SFG) in a waveguide periodically-poled lithium niobate (PPLN) crystal combining the 1319 nm emission line of a neodymium-doped yttrium aluminium garnet (Nd:YAG) laser with an erbium fiber laser at 1030 nm [5]. The generated 578 nm radiation amounts to about 7 mW. The frequency is actively stabilized employing the Pound-Drever-Hall (PDH) method on a 10 cm ultra-stable ULE cavity featureing fused-silica mirrors with ULE compensation rings. The cavity is equipped with a two-stage temperature control using Peltier elements to keep the cavity at the point of vanishing coefficient of thermal expansion (zero CTE). The temperature control system is a digital implementation of the Active Disturbance Rejection Control (ADRC) technique [6]. The radiation is distributed by means of phase-noise cancelled PM optical fiber links with one path going to the ultra-stable cavity, one to the vacuum chamber for spectroscopy and one to a fiber-based optical comb for comparison with the IT-CsF2 SI-second standard. The repumper laser is a commercial pigtail distributed feedback laser emitting at 1389 nm. The output beam focused on the atoms contains 10 mW of light power, broadening the $^3P_0 \rightarrow {}^3D_1$ transition to 300 MHz, while having a frequency stability better than 100 MHz. Therefore active frequency stabilization is not required.

C. Clock cycle

During a single spectroscopy cycle we use around 150 ms of time for cooling and trapping followed by another 100 ms of clock-transition spectroscopy and detection. First atoms are slowed down by counter-propagating a 399 nm light beam

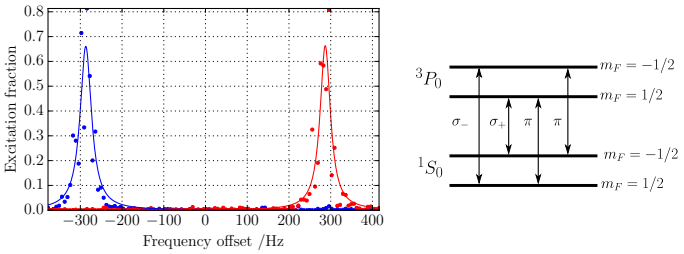

(a) (b)

Fig. 3. a) Scan of the clock transition in the presence of a magnetic field with spin-polarization to the m_F= -1/2 (red) or m_F= +1/2 (blue) hyperfine state b) The hyperfine structure of the $^1S_0 \rightarrow {}^3P_0$ transition in ^{171}Yb

(slower-beam), which is having a power of about 50 mW and a detuning from resonance of -360 MHz. We dispense of a varying magnetic field needed for a Zeeman-slower, but exploit the leaking field of the MOT coils. The six laser beams of the 1st stage MOT add up to about 30 mW of light power with an 1/e radius of 1 cm each and a detuning of -20 MHz. The magnetic field gradient is 0.4 T/m along the z-axis. The duration of slower and 1st stage MOT is 50 ms. The 2nd stage MOT at 556 nm is loaded from the blue MOT with up to 70% efficiency. The six green 2nd stage MOT laser beams amount to a total power of 2 mW with each having an 1/e radius of 0.5 cm. The green MOT is divided in three sub-stages with different frequencies and magnetic field gradients. The first stage (30 ms) is designed for maximum atoms transfer from the blue MOT, implementing a magnetic field gradient of 0.25 T/m. The following 2nd stage (20 ms) utilizes less red-shift and a reduced magnetic field gradient of 0.18 T/m to lower the atomic temperature further. The last stage MOT (10 ms and 0.25 T/m) then only serves to provide an enhanced transfer efficiency of atoms to the lattice. The lattice is formed by a horizontally aligned, retro-reflected and focused 759 nm beam. The laser power on the atoms reaches 1 W in a waist of 45 µm. During on cycle we trap about $2 \cdot 10^3$ atoms with an atomic lifetime in the lattice of 2.7 s. Connected with a dimension of the trapping-area of estimated 0.5 mm we assume an occupation of 1.5 atoms per lattice site. Spin-polarization of the ground state with more than 98% efficency is then applied by a vertically aligned 1 ms green pulse with a magnetic field of $4.12 \cdot 10^{-4}$ T along the same axis. Spectroscopy of the clock transition at 578 nm is executed by a 200 µm focused laser beam collinear to the lattice (laser power about 70 nW) with pulse durations between 50 ms and 100 ms. The resulting clock-level occupation is then determined with 3 resonant 399 nm probe pulses. The first one measures the atoms left in the ground state, the second one reveals the signal background from scattered light and excited hot background gas atoms. The repumper laser at 1389 nm (beam power 10 mW and duration 12 ms) subsequently pumps the excited atoms over the short-lived $^3D_1$ level back to the ground state, where they are detected by the third probe pulse.

III. Results

A. Spectroscopy

Fig. 4 shows the spectra of a single scan over the spin-polarized clock-transition with a Full-Width-Half-Maximum

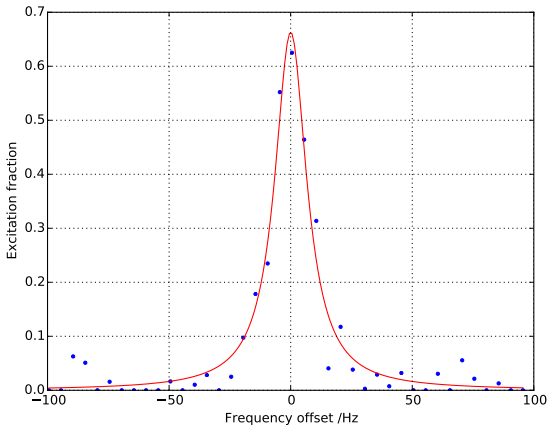

Fig. 4. A single scan (FWHM 16 Hz) over the spin-polarized resonance in the presence of a small magnetic field

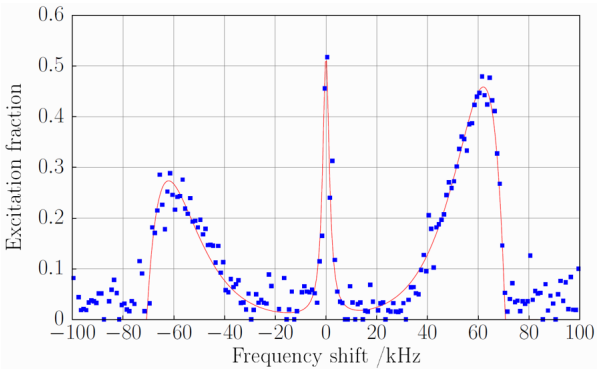

Fig. 5. From the frequency of the red-and blue-sideband's sharp edge the trap depth can be calculated, whereas their shape reveals the thermodynamic temperature and motional state distribution of the atoms

(FWHM) of 16 Hz . During clock-operation the line is typically between 20 Hz and 30 Hz FWHM. In Fig. 5 we observed the spectroscopic signal (blue dots) obtained by interrogation of $1 \cdot 10^4$ atoms in the lattice with 100 μW of light power and a pulse duration of 100 ms. From the fit of the sidebands shape (red curve) we can deduce (for the details of the calculation see [7]) a horizontal trap frequency of 70 kHz corresponding to a trapping depth of 300 Er and an atomic temperature of 4.5 μK. The effect of spin-polarization is shown in Fig. 3a) and a scheme of the clock-transition Zeeman-splitting in Fig. 3b). In order to measure the clock transition frequency we apply a small vertical magnetic field at the position of the atoms, leading to a Zeeman-shift of ca. 300 Hz for each m_F substate.

B. Absolute Frequency Measurement

We obtain the frequency of the unshifted line by alternatingly locking to the $\pm 1/2$ spin-state. In this way the first order Zeeman-shift is sufficiently suppressed by averaging in our measurements. The clock laser is locked to each hyperfine-state atomic resonance by consecutive measurement and stabilization of the excitation fraction in equal distances on the left and right flanks of the transition. Therefore one full clock cycle consists out of four complete spectroscopic cycles and accordingly lasts about one second. We determined the absolute frequency of our clock by using an optical frequency comb that is referenced to a H-maser. The maser on the other hand is being read by our IT-CsF2 fountain clock. We determined the magic wavelength by interleaveing clock cycles with different lattice powers. The stability (Allan-deviation) of one of these measurements is shown in Fig. 6. The measured magic wavelength is 394798228(10) MHz. We determined the linear lattice light shift coefficient to b = −0.0225(3) Hz/(GHz·E_r), in agreement with previous results from other groups [8]. Hyperpolarizability effects were estimated by applying data from [9] and [10] to our situation. With 1.5 atoms per lattice site density shifts need careful evaluation. We determined the density shift by interleaving clock cycles with different blue MOT capture times (45 ms vs. 150 ms). The blackbody-radiation (BBR) shift was calculated by applying the reading of the 10 thermistors to a simple model of the vacuum chamber consisting out of the oven, hot window and aluminum vacuum chamber. The chamber is taken into account as a thermistor-reading adequate environmental temperature with an uncertainty. The oven (400±10°C) and hot window (230±10°C) are modeled as BBR-sources within a certain irradiation angle, which is given by the dimensions of the stainless-stell-junctions to the aluminum chamber. This angle is expanded to an effective angle by including reflections inside the junctions. The greatest contribution to the BBR-shift uncertainty in this calculation originates from the hot window, since its effective angle has a high uncertainty. The first order Zeeman-shift is sufficiently suppressed by reason of averaging in our measurements. Nevertheless higher order effects do appear and need to be evaluated. The magnetic field induced separation of the two m_F states during our clock operation accounts typically to 300(10) Hz in our measurements. We take the results from [9] and apply them to our situation. We determine the magnetic field through the 1st order Zeeman-shift by using $\triangle_{B1} = \alpha_B * B$ and $\alpha_B = 2.10 \cdot 10^3$ Hz/mT to obtain $B = 150(5)$ μT. The 2nd order Zeeman effect is therefore, together with $\gamma_B = -7(1)$ Hz/mT^2, given by: $\nu_{B2} = \gamma_B * B^2 = 0.14(2)$Hz or $2.8(4) \cdot 10^{-16}$ in relative units. The gravitational potential in respect to the geoid at the atoms position is 2336.48(27) m^2/s^2, as determined by a Global Navigation Satellite System/geoid approach [11]. This results in a redshift of 13.474(2) Hz or $2.5997(2) \cdot 10^{-14}$. The probe light shift was evaluated takeing the sensitivity given in [12]. The current uncertainty evaluation of our Yb clock is given in Tab. II. For measureing the absolute frequency of our clock transition we used a working lattice frequency of 394798238 MHz and corrected the ac stark shift accordingly. Preliminary measurements agree with the recommended value established by the BIPM given the current measurement uncertainty. The uncertainty-budget of the Cs-fountain is given in Tab. I.

Effect	Shift×10^{-16}
Zeeman	0.8
Collision	1
Blackbody	0.1
Microwave	1
Redshift	0.1
Total	2.4

TABLE I. IT-CsF2 UNCERTAINTY BUDGET

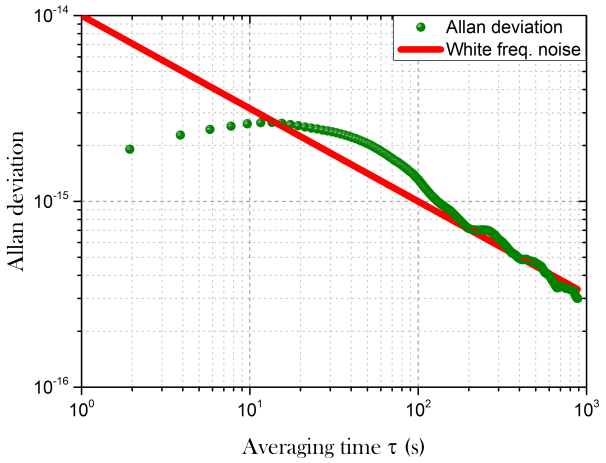

Fig. 6. Allan-deviation of an interleaved measurement featureing alternating low- and high-power lattice to determine the magic wavelength having a stability of about $1 \cdot 10^{-14}/\sqrt{\tau}$

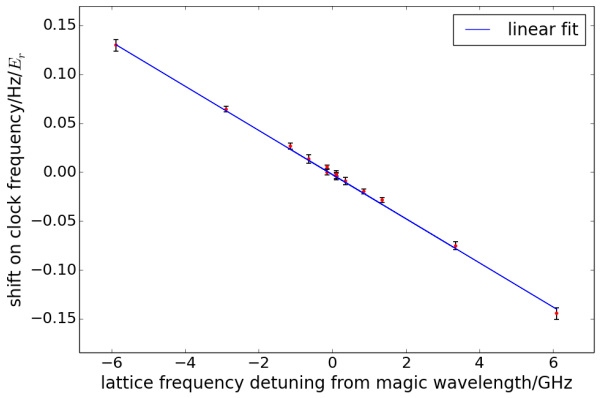

Fig. 7. Determination of magic wavelength. Each point was measured by interleaving high and low light power in the lattice beam. The linear lattice light shift sensitivity coefficient b results as $b = -0.0225(3)$ Hz/(GHz·E_r)

IV. Conclusion

We have completed the Yb clock's physical setup and achieved highly efficient spin-polarization. The characterization of the clock has shown first promising results and a full absolute frequency measurement by comparison towards the IT-CsF2 fountain clock is under way with preliminary results agreeing to the BIPM-recommended value within the stated uncertainty. We have lately replaced the hot window with a cold intra-vacuum mirror. This enables us to reduce the BBR shift uncertainty into the 10^{-17} region and ultimateley the full uncertainty below the 10^{-16}-level. We will also improve our clock laser to raise stability. Our clock will take part in remote as well as local comparisons with other optical clocks within the ITOC (International Timescales with Optical Clocks) project and in stable reference signal distribution via the national fiber link developed under AQUASIM (Advanced Quantum Simulation and Metrology).

Effect	Shift /Hz	Unc. /Hz	Shift$\times 10^{-16}$	Unc.$\times 10^{-16}$
Quadratic Zeeman shift	-0.14	0.02	-2.8	0.4
Lattice Polarizability	-0.16	0.06	3.1	1.2
Hyperpolarizability	0.06	0.02	1.2	0.3
Blackbody shift	-3.2	0.3	-62	6.0
Collisional shift	0.01	0.09	0.2	1.7
Probe light shift	0.0027	0.0012	0.05	0.02
Gravitational red shift	13.474	0.002	259.97	0.02
Total	10.1	0.3	200	6.4

TABLE II. Preliminary uncertainty budget for the Yb lattice clock

Acknowledgment

The authors acknowledge funding from the EMRP Project SIB55-ITOC, MIUR Project PRIN2012 AQUASIM and ITN Marie Curie Project FACT. The EMRP is jointly funded by the EMRP participating countries within EURAMET and the European Union.

References

[1] F. Levi, D. Calonico, C. E. Calosso, A. Godone, S. Micalizio, and G. A. Costanzo, "Accuracy evaluation of itcsf2: a nitrogen cooled caesium fountain," *Metrologia*, vol. 51, no. 3, p. 270, 2014. [Online]. Available: http://stacks.iop.org/0026-1394/51/i=3/a=270

[2] BIPM, *The International System of Units (SI)*, 8th ed. BIPM, 2006.

[3] I. Ushijima, M. Takamoto, M. Das, T. Ohkubo, and H. Katori, "Cryogenic optical lattice clocks," *Nat Photon*, vol. 9, no. 3, pp. 185–189, Mar. 2015. [Online]. Available: http://dx.doi.org/10.1038/nphoton.2015.5

[4] M. Pizzocaro, D. Calonico, P. C. Pastor, J. Catani, G. A. Costanzo, F. Levi, and L. Lorini, "Efficient frequency doubling at 399 nm," *Appl. Opt.*, vol. 53, no. 16, pp. 3388–3392, Jun 2014. [Online]. Available: http://ao.osa.org/abstract.cfm?URI=ao-53-16-3388

[5] M. Pizzocaro, G. A. Costanzo, A. Godone, F. Levi, A. Mura, M. Zoppi, and D. Calonico, "Realization of an ultrastable 578-nm laser for an Yb lattice clock," *IEEE Trans. Ultrason., Ferroelect., Freq. Cont.*, vol. 59, no. 3, pp. 426–431, march 2012.

[6] M. Pizzocaro, D. Calonico, C. Calosso, C. Clivati, G. A. Costanzo, F. Levi, and A. Mura, "Active disturbance rejection control of temperature for ultrastable optical cavities," *IEEE Trans. Ultrason., Ferroelect., Freq. Cont.*, vol. 60, no. 2, pp. 273–280, february 2013.

[7] S. Blatt, J. W. Thomsen, G. K. Campbell, A. D. Ludlow, M. D. Swallows, M. J. Martin, M. M. Boyd, and J. Ye, "Rabi spectroscopy and excitation inhomogeneity in a one-dimensional optical lattice clock," *Phys. Rev. A*, vol. 80, p. 052703, Nov 2009. [Online]. Available: http://link.aps.org/doi/10.1103/PhysRevA.80.052703

[8] Z. W. Barber, J. E. Stalnaker, N. D. Lemke, N. Poli, C. W. Oates, T. M. Fortier, S. A. Diddams, L. Hollberg, C. W. Hoyt, A. V. Taichenachev, and V. I. Yudin, "Optical lattice induced light shifts in an Yb atomic clock," *Phys. Rev. Lett.*, vol. 100, p. 103002, Mar 2008. [Online]. Available: http://link.aps.org/doi/10.1103/PhysRevLett.100.103002

[9] N. D. Lemke, A. D. Ludlow, Z. W. Barber, T. M. Fortier, S. A. Diddams, Y. Jiang, S. R. Jefferts, T. P. Heavner, T. E. Parker, and C. W. Oates, "Spin-1/2 optical lattice clock," *Phys. Rev. Lett.*, vol. 103, no. 6, p. 063001, Aug 2009.

[10] N. Nemitz, T. Ohkubo, M. Takamoto, I. Ushijima, M. Das, N. Ohmae, and H. Katori, "Frequency ratio of yb and sr clocks with 51017 uncertainty at 150seconds averaging time," *Nat Photon*, vol. advance online publication, pp. –, Feb. 2016. [Online]. Available: http://dx.doi.org/10.1038/nphoton.2016.20

[11] H. Denker, C. Voigt, and L. Timmen, "Private communication," 2016.

[12] N. Poli, Z. W. Barber, N. D. Lemke, C. W. Oates, L. S. Ma, J. E. Stalnaker, T. M. Fortier, S. A. Diddams, L. Hollberg, J. C. Bergquist, A. Brusch, S. Jefferts, T. Heavner, and T. Parker, "Frequency evaluation of the doubly forbidden $^1S_0 \rightarrow {}^1P_3$ transition in bosonic ^{174}Yb," *Phys. Rev. A*, vol. 77, no. 5, p. 050501, May 2008. [Online]. Available: http://pra.aps.org/abstract/PRA/v77/i5/e050501